
This is an electronic reprint of the original article.
This reprint may differ from the original in pagination and typographic detail.

Viitala, Raine; Widmaier, Thomas; Hemming, Björn; Tammi, Kari; Kuosmanen, Petri

Uncertainty analysis of phase and amplitude of harmonic components of bearing inner ring four-point roundness measurement

Published in:
Precision Engineering

DOI:
[10.1016/j.precisioneng.2018.05.008](https://doi.org/10.1016/j.precisioneng.2018.05.008)

Published: 01/01/2018

Document Version
Publisher's PDF, also known as Version of record

Published under the following license:
CC BY-NC

Please cite the original version:
Viitala, R., Widmaier, T., Hemming, B., Tammi, K., & Kuosmanen, P. (2018). Uncertainty analysis of phase and amplitude of harmonic components of bearing inner ring four-point roundness measurement. *Precision Engineering*, 54, 118-130. <https://doi.org/10.1016/j.precisioneng.2018.05.008>

This material is protected by copyright and other intellectual property rights, and duplication or sale of all or part of any of the repository collections is not permitted, except that material may be duplicated by you for your research use or educational purposes in electronic or print form. You must obtain permission for any other use. Electronic or print copies may not be offered, whether for sale or otherwise to anyone who is not an authorised user.



ELSEVIER

Contents lists available at ScienceDirect

Precision Engineering

journal homepage: www.elsevier.com/locate/precision

Uncertainty analysis of phase and amplitude of harmonic components of bearing inner ring four-point roundness measurement

Raine Viitala^{a,*}, Thomas Widmaier^a, Björn Hemming^b, Kari Tammi^a, Petri Kuosmanen^a

^a Aalto University, School of Engineering, Department of Mechanical Engineering, Finland

^b MIKES Metrology, VTT Technical Research Centre of Finland Ltd, Finland

ARTICLE INFO

Keywords:

Monte-Carlo simulation
Phase uncertainty
Harmonic component uncertainty
Uncertainty evaluation
Bearing excitation
Odd and even harmonic components
Four-point method
Three-point method

ABSTRACT

The four-point roundness measurement method enables the measurement of roundness without a requirement for a precise rotating motion of the workpiece or a measurement sensor. The four-point roundness measurement method can separate the roundness profile and the motion of the rotating axis of the workpiece. In the present study, the uncertainty of the four-point roundness measurement of a bearing inner ring was analysed. The bearing inner ring was installed in its operating position on the shaft of a large rotor during the measurement in order to investigate the bearing inner ring roundness profile in operating conditions. Since the measurement evaluation using the four-point method is complex, the uncertainty analysis was conducted through a Monte-Carlo simulation, using realistic error sources in typical measurement conditions. The uncertainty of both the amplitude and phase of the harmonic components of the roundness profile was analysed for the 2nd till the 30th harmonic component. Attention was directed especially towards the phase of the harmonic components, since the uncertainty of the phase is analysed very little in existing research studies. In addition, the phase of the harmonic components of the roundness profile is important when considering compensative precision grinding applications of round workpieces. The results show that below the 10th harmonic component, the maximum amplitude standard uncertainty was circa 0.5 µm, and the maximum phase standard uncertainty was circa 5°. The standard uncertainties of the amplitudes for the complete harmonic component range were below 1.3 µm for odd components and 0.2 µm for even components. The maximum standard uncertainties of the phases for the complete harmonic component range were circa 15° for odd components and circa 5° for even components. The measured roundness profile itself did not have an effect on the uncertainty of the method.

1. Introduction

Roundness is a key quality measure of rotating components (i.e., rotors) in many fields of machinery, such as turbines, electric motors and rolls in the paper, steel and non-ferrous metal manufacturing industries. The rotational accuracy of a rotor is greatly affected by the bearings, which are core components of a rotor system. The bearings support the rotor during rotation and sustain the forces exerted by the rotor and external loads. Additional rotational error sources can be unbalance, bending stiffness variation and roundness errors of the rotor itself. Bearings are typically not tailored for a specific rotor, but they are considered as replaceable separate components. The roundness errors of the bearing components can deviate the motion of the rotor central axis as well as cause undesired subcritical resonance vibration of the rotor [1,2].

Typical bearing arrangement is a rolling element bearing with an outer ring connected to the foundation through the bearing housing,

balls or rollers as rolling elements and an inner ring attached to the rotor shaft. The bearings excite vibrations into the rotor: the inner ring, outer ring and rolling elements have geometrical errors, which cause harmful vibration with a frequency proportional to the rotating frequency of the rotor. The most remarkable bearing element excitations are caused by the roundness profile of the bearing inner ring, which is attached to the rotor and rotates at the same frequency. The inner ring roundness profile is a sum of the inner ring and the possible conical adapter sleeve thickness variations and the roundness of the shaft (Fig. 1), on which the bearing is attached. Thus, the final bearing inner ring roundness profile is a property of the bearing assembly on the rotor shaft. The roundness errors are commonly presented as harmonic components of the Fourier series.

ISO standard 12181 [3,4] defines roundness as a feature of a circular cross-section of an object. Moreover, the diameter of a round object is typically measured as a two-point measurement, which is sensitive to the out-of-roundness of the measured object. If knowledge

* Corresponding author. Aalto University School of Engineering, Dept. of Mechanical Engineering | Engineering Design, Sähkötieteenkatu 4P, PL 14400, 00076 Aalto, Finland.
E-mail address: raine.viitala@aalto.fi (R. Viitala).

<https://doi.org/10.1016/j.precisioneng.2018.05.008>

Received 20 April 2018; Received in revised form 14 May 2018; Accepted 22 May 2018

0141-6359/© 2018 The Authors. Published by Elsevier Inc. This is an open access article under the CC BY license (<http://creativecommons.org/licenses/by/4.0/>).

Nomenclature

A	Amplitude	N	Normal distribution
c	circa, approximately	P	Phase
D	Even harmonic components of the roundness profile	PDF	Probability distribution function
E	Odd harmonic components of the roundness profile	STD	Standard deviation
FFT	\mathcal{F} Fast Fourier Transform	S1 – S4	Sensors S1, S2, S3 and S4 in four-point roundness measurement method
G	Combined harmonic components from two-point and three-point methods	U	Uncertainty
GUM	Guide to the expression of uncertainty in measurement	UPR	Undulations per revolution
m	Roundness profile measured with Ozono three-point method	Δr	Diameter variation profile measured with two-point method
n	Lobe number, harmonic component number	μ	Mean
		σ	Standard deviation

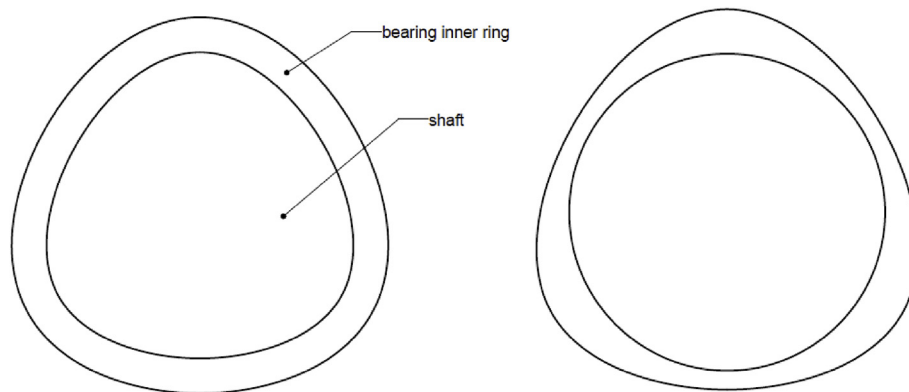


Fig. 1. Schematic visualizing the formation of the roundness error of an installed bearing inner ring. On the left hand side, the roundness error (in this case the 3rd harmonic component, triangularity) is caused by the roundness error of the shaft, on which the relatively thin inner ring has been tightened and thus deformed. On the right hand side, the roundness error is caused by the triangular thickness variation of the bearing inner ring. In reality, the roundness error is a composition of both these error types.

of the shape of the roundness error or the harmonic components of the roundness profile are needed for the application, roundness profile measurements are essential [5–7].

Certain harmonic components of the roundness profile of a bearing inner ring can cause harmful subcritical resonance vibration in the operating range of a large rotor. The harmful subcritical resonances are observed, when the bearing inner ring excites the rotor at its natural frequency. For example, triangular (3rd harmonic) roundness error in the bearing inner ring excites the rotor three times per revolution leading to subcritical resonance at $1/3$ of the natural frequency, with quadrangular (4th harmonic) roundness error at $1/4$ of the natural frequency etc. The amplitude of the harmonic components of the roundness error has a substantial effect on the vibration amplitudes [1,2].

Commercial roundness measuring machines are available for laboratory-scale measurements (diameter typically below 500 mm, length typically below 1000 mm). They typically utilize only one sensor for measuring the roundness profile, since the high-accuracy bearing of the roundness measuring machine confirms the accurate rotating motion of the workpiece. However, these machines cannot be used for large-scale rotor and bearing measurements due to the size of the objects. For example, rotors in the paper industry have diameters of over 1000 mm and a length of several meters up to 12 m. The roundness of slightly larger components can be measured with coordinate measuring machines, but the measurement uncertainty is larger than with roundness instruments.

Multipoint roundness measurement devices are typical in the paper and in the steel industry, where the roundness of the rolls is important for the quality of the end product. The measurement setup cannot prevent the rotational error of the centreline of the roll, and thus multipoint methods have to be used. Most of these roll roundness measurement applications rest on a three-point Ozono method, which uses three weighted sensor signals to calculate the roundness [8]. The control systems of the modern roll grinding machines enable the usage of the measured roundness profile for error compensation in the

grinding process, where the roundness error has to be minimized [9–13]. Another multipoint method for spindle run-out separation is presented by Ref. [14]. In their study, the measurement system is implemented to measure the run-out of the spindle of a high precision turning lathe, and finally the roundness of the achieved workpiece.

The reliability of the measurement revealing the harmonic components of the roundness profile of an installed bearing inner ring is important for the manufacturing and quality control process of rotors with excellent dynamic properties.

Measurement uncertainty can be estimated with the GUM (Guide to the expression of uncertainty in measurement) method using a linear Taylor series [15]. The GUM method is fairly unambiguous and used commonly if the measurement method and model is simple, linear and well defined. However, for more complex measurements models, it is challenging to establish the sensitivity coefficients.

The GUM method was extended by applying Monte-Carlo simulations to evaluate the uncertainty [16]. The Monte-Carlo simulations enabled the introduction of randomised input quantities and the evaluation of their contributions to the measurement uncertainty. The benefit of the method is in using the true measurement model to evaluate the uncertainty, and thus a non-linear measurement model can be used [17–19].

The phase of the harmonic components of the roundness profile, or the uncertainty of the phase, has received little attention in previous research. However, the phase of the harmonic components is significant, when considering, for example, applications, where the roundness profile measurement data is used as a feedback for the precision manufacturing procedure (such as 3D predictive grinding for round workpieces, presented, e.g., by Kuosmanen [12]). The phase error of the harmonic component can affect the interpreted roundness profile in a way, which essentially doubles the error, when used as feedback data for the precision manufacturing process.

This paper presents a method to measure the roundness profile of a bearing inner ring, which is installed on a rotor shaft during the

measurement. The roundness profile was measured using a four-point method, which is able to separate the central axis movement and the roundness profile of the workpiece. Furthermore, the Monte-Carlo approach to measurement uncertainty analysis was used to estimate the measurement uncertainty of the measurement method. Particular consideration in the present study is directed to the phase uncertainty of the harmonic components of the roundness profile. The method is presented and applied to the bearing inner ring roundness analysis, and the results are presented and discussed.

2. Methods and material

2.1. Fourier series and roundness

The Fourier series can represent the roundness profile, describing the magnitude and the order of the waveforms deviating from the ideal circular shape. In the series, the second order ($n \geq 2$) and higher terms are relevant. The zeroth order describes the offset and the first order describes the eccentricity; both of them can be compensated by adjusting the origin, and thus are not considered as part of the roundness profile. The visual representation of roundness profiles is typically made by using polar coordinates.

The fast Fourier transform (FFT) algorithm to transform a time-domain signal into the frequency-domain representation was initially presented by Cooley and Tukey [20]. The undesired components can be filtered simply in the frequency domain by manipulating the frequency domain coefficients (see, e.g., [21]). The FFT algorithm is used for both identifying and filtering the harmonic components in our research. With the usage of the FFT, the amplitudes and phases of the harmonic components of the roundness profile can be identified.

2.2. Roundness measurement with four-point method

The four-point roundness measurement used in this study has been designed to combine the two-point diameter variation measurement and the Ozono three-point roundness measurement. The methods are presented below.

The two-point method (Fig. 2, sensors S1 and S4) can be used to measure diameter variation profiles or absolute diameters, if the distance between the probes is known. However, this method cannot be used for roundness profile measurements, since it suffers from harmonic filtration: odd waviness components (e.g., 3-lobe) cannot be separated from the motion of the workpiece central axis. With even lobe shapes, such a problem does not exist [9,13,22–24].

The derivation of the diameter variation profile from the two-point method measurements is straightforward. It only includes the summation (addition or subtraction) of the probe signals. The equations are presented, for example, by Widmaier et al. [24].

The three-point roundness measurement method presented by Ozono [8] is one of the first numerical multipoint methods for roundness evaluation. The Ozono three-point method utilizes three run-out signals (Fig. 2, sensors S1, S2 and S3) measured from the workpiece surface. It is able to separate the central axis movement accurately. The three-point method does not suffer from the major harmonic filtration when the lobe number is below 35 and sensor angles 0° , 38° and 67° are used. To optimize the method for other lobe number ranges, different sensor angles should be used [14,25,26]. The method is complex, and the simplified equations are presented, for example, by Widmaier et al. [24].

As mentioned earlier, the two-point method suffers from harmonic filtration making it unable to detect odd-numbered harmonic lobes in a roundness profile [9,23]. However, even-numbered harmonics are detected accurately. A multi-point measurement method commonly used for roll geometry measurements [24] is the hybrid four-point method, which combines the three-point Ozono method with the two-point method. The hybrid four-point method originally presented by

Väänänen [27] and further analysed by Widmaier et al. [24] uses the three-point method for odd harmonic component measurement and the two-point method to measure even numbered lobes. The measurement results are then combined together. The combined result has been found to be more accurate than results from one method alone [24,27]. The idea to combine harmonic components from separate measurement methods has been stated in the roundness standards calibration as well [28].

Fig. 3 shows how to use the hybrid-method to extract the harmonic components of the roundness profile. The roundness profiles produced by both the two- and three-point method are Fourier transformed to obtain the amplitudes and phases of the harmonic components. The even components are selected from the two-point method, whereas the three-point method produces the odd components. This dataset represents the final distribution of amplitudes and phases of the harmonic components in the roundness profile.

2.3. Measurement device

2.3.1. Measurement device framework

The measurement frame was machined of aluminium. The fittings for the sensors were manufactured carefully without detaching the frame in the machine tool in between in order to minimize angular errors. The thermal expansion properties of aluminium are not optimal, but the problem was considered insignificant due to the short measurement time (less than 30 s). A rig made of aluminium profiles supported the frame.

2.3.2. Probes

Digital length gauges (Heidenhain MT12) were used. The working principle of these sensors comes from the photoelectric scanning of a grated measurement standard. The sensors have a plunger with a ball head for tactile probing. The accuracy of the length gauges was verified

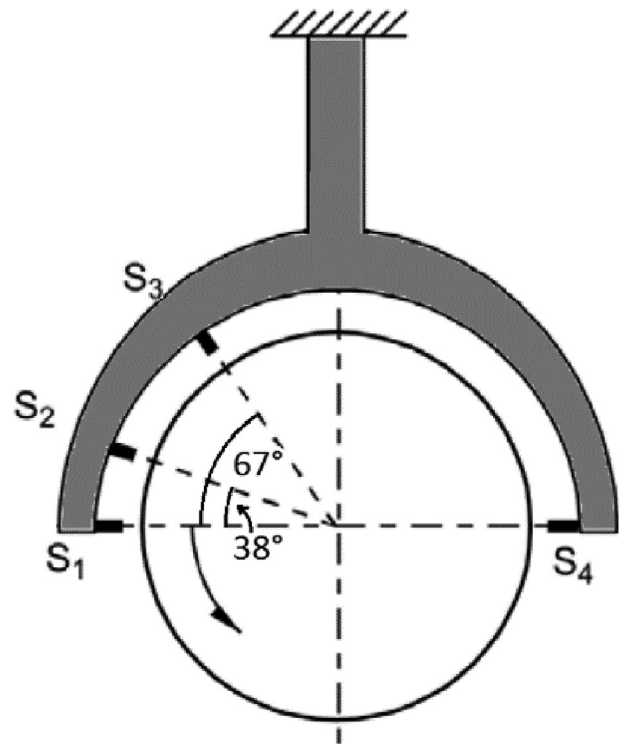
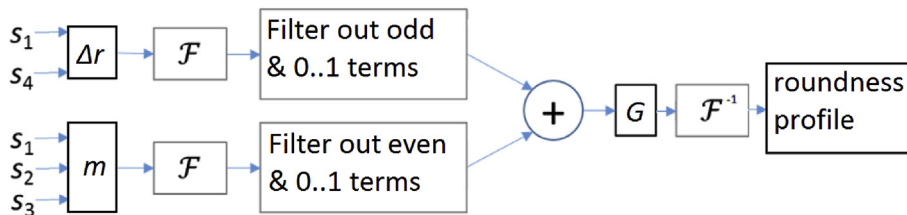


Fig. 2. Probe orientations in a four-point roundness measurement system. Probes S1 and S4 are used with the two-point method. Probes from S1 to S3 are used with the Ozono three-point method. In the four-point method, all four probes are utilized.



method and odd components from the three-point method. With inverted FFT (\mathcal{F}^{-1}) the measured roundness profile can be reconstructed.

to stay within $\pm 0.2 \mu\text{m}$ by interferometric calibration at VTT MIKES, which is the national metrology institute of Finland.

2.3.3. Measurement setup

The measurement setup (Fig. 4) consisted of a measurement frame with four probes attached to it and a bearing inner ring, which was measured while installed on the rotor shaft. This measurement method reveals the roundness profile of the bearing inner ring in operating conditions. The rotor was supported by separate rollers, since the bearing was measured, and thus could not support the rotor.

2.3.4. Calibration profile and disc

A calibration disc with a roundness profile consisting of harmonic components from 2 to 30 UPR (undulations per revolution) was manufactured previously in earlier research (Fig. 5, [9]). The roundness deviation was minimized by optimising the phase angles of the individual harmonic components.

Naturally, due to the manufacturing accuracy, the geometry of the realised disc differed from the designed geometry by a few micrometres. The design process and the measurements of several calibration discs, including the particular disc presented here, can be found in Refs. [29,30]. The calibration disc roundness profile measured with the four-point method and with a reference device were compared, suggesting a less than $1 \mu\text{m}$ difference in harmonic amplitudes [24].

Due to the previous use of the calibration profile (Fig. 5) and the comparability of the results, the calibration profile was used as an input for the four-point algorithm in the present study as well. In addition to the phase distribution of the calibration profile, different phase distributions were randomly generated. These random phase distributions were used to analyse the effect of the phase of the harmonic components on the results of the roundness measurement.

Fig. 3. Schematic of the principle of combining two-point (Δr) and Ozono three-point (m) methods. FFT (\mathcal{F}) is utilized to filter out odd and even harmonic roundness components in two- and three-point measurements. The 0^{th} and 1^{st} terms are filtered out as well, since they are not used to calculate the roundness profile. Finally, the results are combined to reveal the final harmonic roundness components (G), containing even components from the two-point

2.4. Simulation based uncertainty evaluation

Uncertainty budgets and uncertainty evaluation have typically been used to recognise and analyse individual uncertainty and error sources affecting the overall uncertainty of the method. Typical GUM uncertainty analysis collects uncertainty components and sensitivity coefficients into a table. The Monte Carlo approach does not have a direct counterpart for sensitivity coefficients, but the task can be imitated with Monte Carlo simulations. The method is to execute the Monte Carlo simulation with respect to one error source at a time and fix the others at their best estimates. The supposed sensitivity coefficients can then be characterised from the Monte Carlo simulation results [31].

In the present study, the uncertainty of the four-point roundness measurement of a bearing inner ring installed on a rotor shaft was evaluated. The principle for the Monte Carlo based uncertainty evaluation was to produce artificial roundness measurement data, which was biased with appropriate distributions of error contributions. A Python program was used to input a large number of this artificial biased roundness measurement data into the four-point algorithm. The procedure was as follows:

1. The calibration profile (Fig. 5) was used as input.
2. The input signals from S1 to S4 artificially measuring the calibration profile were distorted mathematically based on realistic distributions of error sources.
3. The distorted input signals were fed to the four-point algorithm.
4. The four-point algorithm (Fig. 3) calculated the amplitudes and phases of the resulted roundness profile
Steps from 1 to 4 iterated 100000 times
5. The means and standard deviations of the resulted amplitudes and the circular means and circular standard deviations of the resulted phases of the harmonic components were calculated.



Fig. 4. Bearing inner ring measurement setup. The bearing inner ring was measured, while installed on the rotor shaft. Other bearing components, such as roller elements, roller element holders and outer ring were uninstalled prior to the measurement. During the measurement, the rotor was supported with two additional rollers.

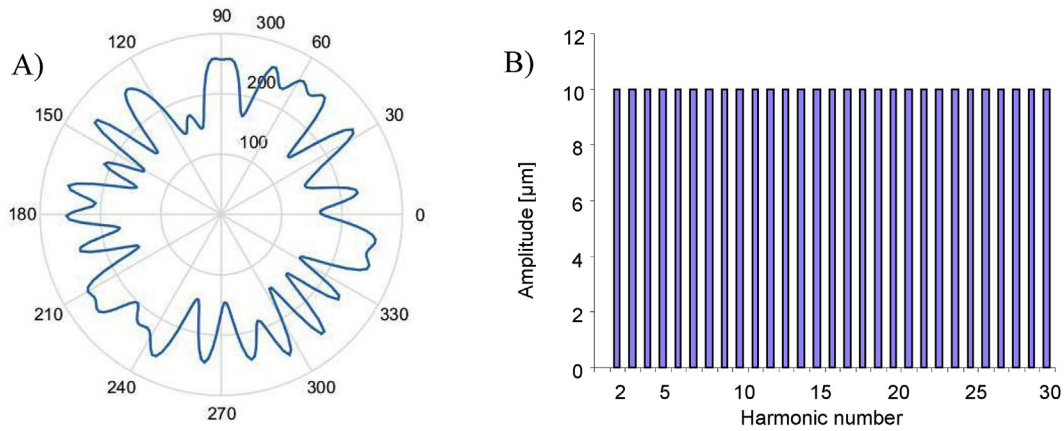


Fig. 5. A) Designed calibration disc profile with harmonic components from 2 to 30 undulations per revolution. This profile was used in the present study as well to estimate the uncertainty of the measurement method. B) The amplitudes of the harmonic components were all 10 μm . The phases were optimised to minimize the roundness error [24].

2.4.1. Error sources

The error sources and their probability distribution functions (PDF) are presented in the four-item list below. The chosen error sources and their uncertainty contributions are based on the experiences of authors in these types of measurements. The PDFs of all error sources were assumed to be normally distributed.

1. Scale error of the probes. Based on the VTT Mikes calibrations experience, a standard uncertainty of 0.3 μm was assumed for the scale error of the probes. The error was randomly generated separately from the error distribution for each measured point of the artificial roundness measurement.
2. The angular position of the probes (Fig. 6). In the three-point Ozono part of the four-point measurement, the angular positions should be 0°, 38°, 67° or 180° in polar coordinates (Fig. 2). Väänänen [27] and Kato et al. [25,26] suggested that the method is sensitive to these angles. Based on the manufacturing accuracy of the frame (Fig. 4), the positions of the probes were assumed to vary from their theoretical angular positions with a standard uncertainty of 0.25°. The error was randomly generated from the error distribution once for each probe during each artificial roundness measurement, i.e., the angle was not assumed to vary during the measurement.
3. The vertical position of the frame (y-axis error) (Fig. 6). The position of the measurement frame in a vertical direction may vary between measurements, i.e., the point, where the probe axes intersect each other does not coincide with the central axis of the roundness profile. It was assumed, that the vertical position of the measurement frame had an error with a standard uncertainty 0.25 mm. The 0° and 180° probes were used to position the frame precisely in a horizontal direction (x-direction). The error was randomly generated from the error distribution once during each artificial roundness measurement, i.e., the y-position was not assumed to vary during the measurement.
4. Temperature error (Temperature change of the frame). The

temperature of the frame was assumed to change with a standard uncertainty of 0.5 °C. The temperature of the frame was assumed to change linearly without hysteresis during the measurement from the initial value (20 °C) to the final value randomly generated from the error distribution. The effect of the thermal error was modelled as a linear thermal expansion of the frame (the frame shape remained unchanged). The origin of the expansion was the centre of the frame, where the sensor axes intersect.

Table 1 presents the error contributions. Due to the scale error and angular position error being calculated separately for each probe, the overall number of different error contributions is 10.

The sensitivity of the error sources was analysed by running the simulation one error at a time. In the sensitivity evaluation, the standard deviations of the error sources were increased to 1.0 μm (scale error), 0.5° (angular position error), 0.5 mm (vertical position error) and 1.0 °C (temperature error).

3. Results

The following presents the results produced by the Monte Carlo simulation. Both amplitudes and phases produced by the simulated measurements are presented. The amplitudes are presented as such. The phases are normalized, i.e., the difference between the mean value and the original value is shown. In the figures, the uncertainty of each harmonic component is represented by error bars.

In addition, it must be noted, that the phase values and their uncertainties are expressed in the coordinate system of the corresponding harmonic component in question. E.g., the 30th harmonic component represents undulations, which occur 30 times per revolution. The angular period of the 30th harmonic is thus $360^\circ/30 = 12^\circ$ in the workpiece coordinates. If there is a need to analyse the phase values and their uncertainties in the workpiece coordinates, the values must be divided by the harmonic component number in question.

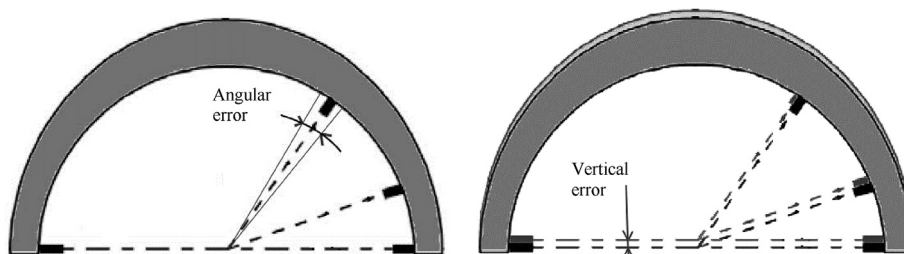


Fig. 6. Left: Angular position error of the probe. Right: Vertical position error of the frame.

Table 1
Error sources and their statistical distributions (notation following [16] in the present study.

Error source	PDF	Parameters	
		μ	σ
1. Scale error of the probe	$N(\mu, \sigma^2)$	0 μm	0.3 μm
2. Angular position error of the probe	$N(\mu, \sigma^2)$	0°	0.25°
3. Vertical position error of the frame	$N(\mu, \sigma^2)$	0 mm	0.25 mm
4. Temperature error	$N(\mu, \sigma^2)$	20 °C	0.5 °C

3.1. All error sources

Fig. 7 shows the results of the simulation with all the different error sources specified in Chapter 2.4.1. Generally, the mean of the measured harmonic components had only small variations. The mean of the even component amplitudes decreased with increasing harmonic number. However, the uncertainty of the harmonic components varied substantially in both amplitude and phase results. The uncertainty of the phases of the even harmonics grew almost linearly with increasing harmonic number. The odd harmonic components produced significantly greater uncertainties than the even harmonic components. The difference is notable especially in amplitude uncertainties.

The maximum standard uncertainties were 1.31 μm (27th) and 15.73° (29th).

3.2. Sensitivity: scale error of the probes

The sensitivity of the method to the scale error of the probes is presented in Figs. 8–11. The mean of the simulation results accurately represented the input values of the algorithm. In addition, the scale error did not have a substantial effect on the phase detected by the method. Altogether, the scale error had little effect on the uncertainties of the amplitudes considering the overall uncertainties presented in Fig. 7. The maximum uncertainty of 0.12 μm (13th) was produced by S2.

S1 error contributed to both odd and even harmonic uncertainties, since it is used in the calculation of both of them. S4 error contributed only to the even harmonic uncertainties, since it is used only for their calculation. S1 and S4 both produced similar 0.04 μm uncertainty for even harmonics. Consequently, S2 and S3 contributed only to odd harmonic uncertainties, since they are not used in the even harmonic calculation. S2 error produced greater uncertainties than S3.

3.3. Sensitivity: angular position error of the probes

The sensitivity of the measurement method to the angular position error of the probes is presented in Figs. 12–15. The mean of both the amplitudes and phases represented the input values quite accurately. Some minor outliers were detected in the higher harmonics (higher than 25th). The highest mean amplitude error was 0.27 μm (S1, 29th) and the highest mean phase error was 1.37° (S3, 25th).

The angular position error had practically no effect on the amplitude uncertainties of the even harmonic components, i.e., components measured only utilizing sensors S1 and S4, and thus the S4 angular position error caused no substantial amplitude uncertainties at all. However, the angular position errors in S1, S2 and S3, which were used in the odd harmonics calculation, caused some substantial amplitude uncertainties, the highest uncertainty being 1.99 μm (S2, 27th).

The angular position error of the probes caused significant phase uncertainties for both even and odd harmonic components. Generally, the phase uncertainty was higher with increasing harmonic number. S2 and S3 errors produced an effect on the phases of the odd harmonic components only. The effect of S2 error was significantly higher in certain components, the highest uncertainty being 14.45° (S2, 29th). S1 error affected both the phases of the even and the odd harmonics. However, the phase uncertainties of the odd harmonics were smaller than those of S2 or S3 errors. S1 and S4 errors produced similar phase uncertainties for even harmonics. The phase uncertainties of the even harmonics increased almost linearly with the increasing harmonic number.

3.4. Sensitivity: vertical position error of the frame

The sensitivity of the measurement method to the vertical position error of the frame is presented in Fig. 16. The mean values of both the amplitude and the phase of the harmonic components were detected quite accurately. However, some outliers were observed, the largest being 0.34 μm and 1.39° (both 25th). The phase of the even components was not affected by the error at all, considering both the mean and the uncertainty.

The uncertainty of the phase of the odd components had local maximums at harmonic numbers 9, 19 and 29. The largest uncertainty of the phase was 25.82° (29th).

The uncertainty of the amplitudes was substantial in consideration of certain harmonic numbers, the maximum amplitude uncertainty being 1.15 μm (25th).

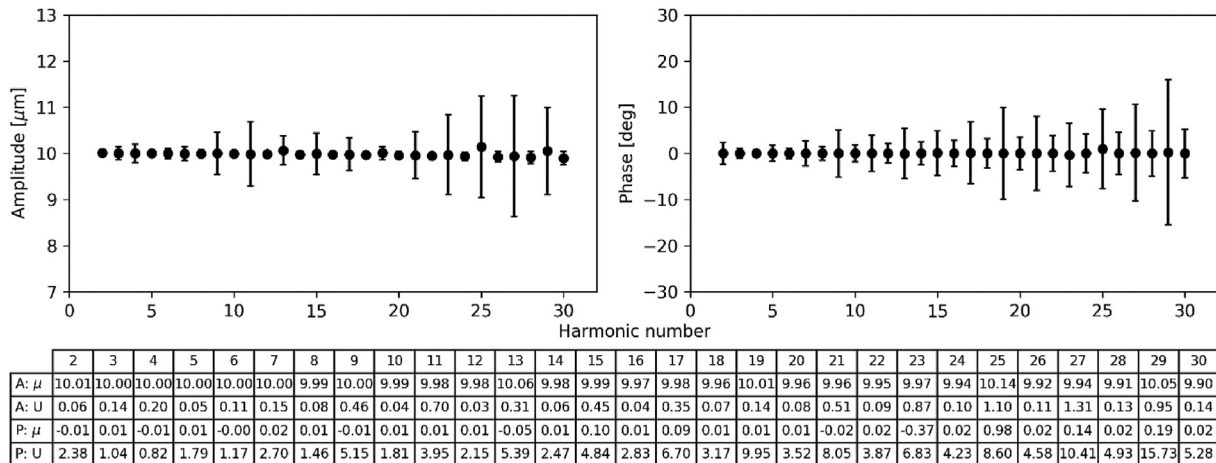


Fig. 7. Simulation output with all error sources (quantities presented in Table 1) and 100000 iterations. Phases are normalized, i.e., the difference between the mean value and the original value is shown.

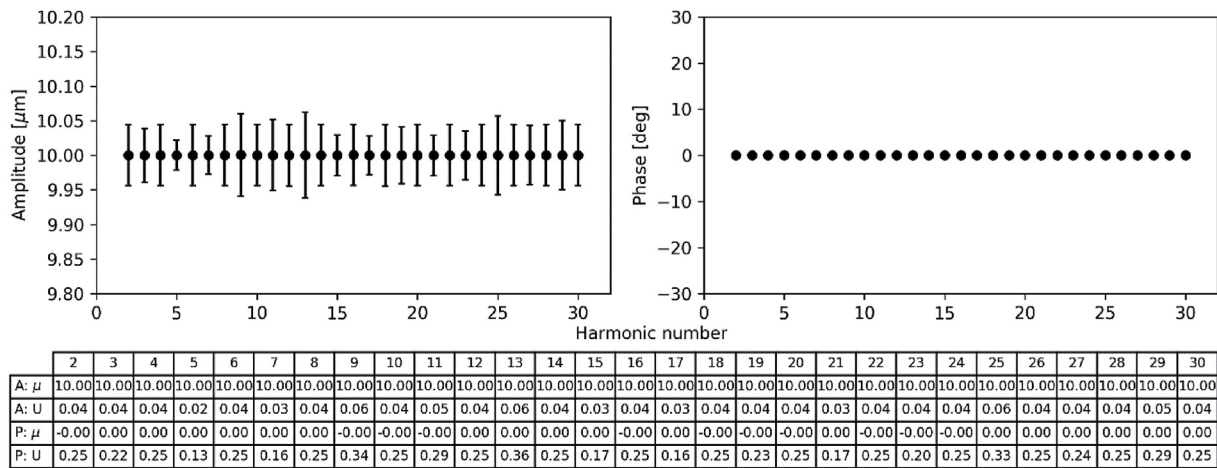


Fig. 8. Simulation output with only S1 scale error (1 μm STD) and 100000 iterations. Other error sources were set to zero. Phases are normalized, i.e., the difference between the mean value and the original value is shown.

3.5. Sensitivity: temperature error

The sensitivity of the measurement method to the temperature error is presented in Fig. 17. The mean of both the amplitude and the phase were detected to be similar to the input values.

The amplitude and phase uncertainties were small. However, unlike other cases, the temperature error caused the largest amplitude uncertainties in the lower order harmonics. The highest uncertainty was 0.39 μm (4th). The highest phase uncertainty was 4.69° (2nd). Altogether, the temperature error affected the even harmonics more than the odd harmonics.

3.6. Sensitivity: random phases of the input profile

Fig. 18 presents the results that investigate the sensitivity of the four-point method to the phases of the harmonic components of the roundness profile being measured. The phases of the harmonic components of the input profile were randomly generated and thus different in each case. The amplitudes were 10 μm for all the harmonic components from 2 to 30, as in the previous tests. Notable differences in the means or uncertainties of the harmonic components were not detected. Moreover, the results are the same as in Fig. 7 in which the calibration profile with optimized phase distribution was used as an input roundness profile.

4. Discussion

The result shown in Fig. 7 presents the uncertainty estimates of the roundness measurement method when all the error sources discussed in Chapter 2.4.1 were applied in the simulation. These error sources (probe scale, probe position, frame position and temperature) with the specified uncertainties are the best estimate of the typical measurement conditions. The means of both the amplitude and the phase of the harmonic components of the roundness profile were detected accurately.

The maximum uncertainty of the amplitudes was c. (circa) 0.5 μm , in relation to the lower order harmonic components (below 10th). These are of interest, when considering the effect of the bearing inner ring roundness error on the dynamic behaviour of a large flexible rotor. The overall maximum uncertainty of the amplitudes of the harmonic components was c. 1.3 μm for odd components and c. 0.2 μm for even components.

The uncertainty of the phases increased significantly in certain harmonic components. Below the 10th harmonic component, the maximum was c. 5°. The overall maximum was as high as c. 16° for odd components and c. 5° for even components. However, as described in Chapter 3, the phase values and their uncertainties are presented in the coordinate system of the harmonic component in question. The phase uncertainty of a certain harmonic component in the workpiece coordinate system is calculated by dividing the value by the harmonic

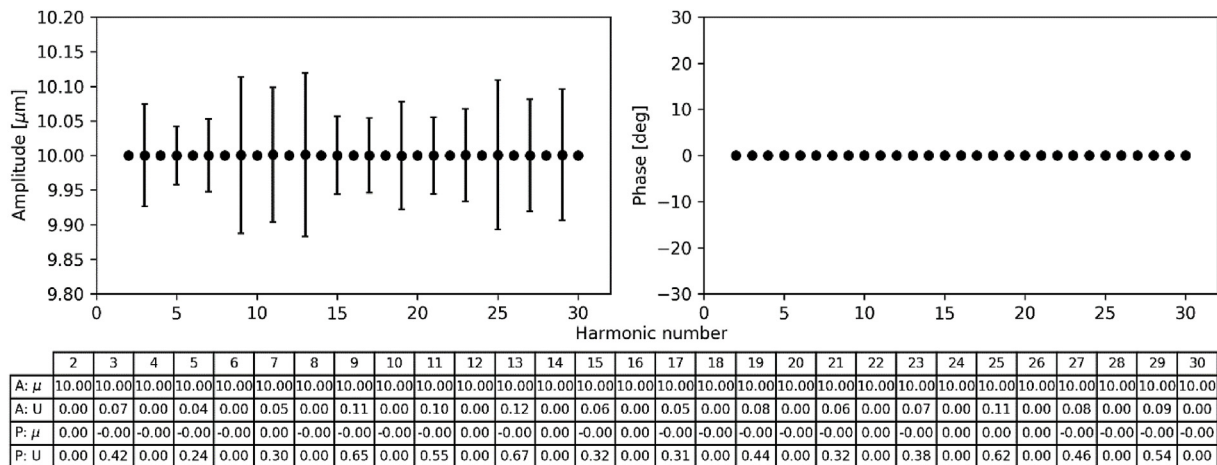


Fig. 9. Simulation output with only S2 scale error (1 μm STD) and 100000 iterations. Other error sources were set to zero. Phases are normalized, i.e., the difference between the mean value and the original value is shown.

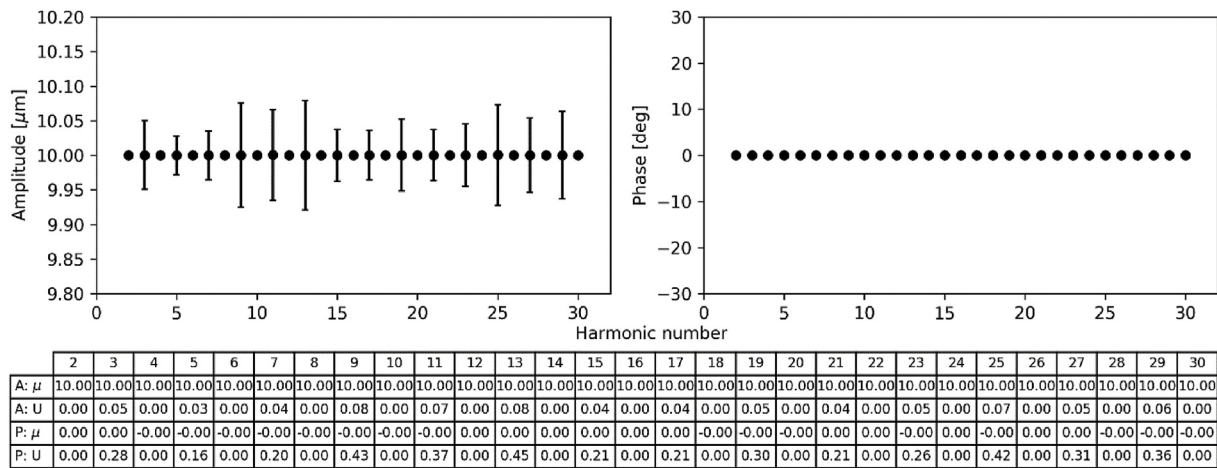


Fig. 10. Simulation output with only S3 scale error (1 μm STD) and 100000 iterations. Other error sources were set to zero. Phases are normalized, i.e., the difference between the mean value and the original value is shown.

number, e.g., 15.73° uncertainty at 29th component denotes $15.73^\circ / 29 = 0.54^\circ$ in the workpiece coordinates. Consequently, the phase uncertainties rising with the harmonic component may be misleading, if this issue is not concerned.

4.1. Odd and even harmonic components

The odd harmonic components produced generally higher uncertainties than the even components in both the amplitudes and the phases. The reason is in the combination of two different measurement methods: the odd harmonic components were measured utilizing the Ozono three-point method and the even with the two-point method.

4.2. Scale error of the probes

The results suggest that the four-point method is insensitive to the scale error of the probes. The scale error of the sensors used in the research (Heidenhain MT12) contributed only a little to the overall uncertainties of the amplitudes. The phases were not affected at all.

The small cosine type alignment errors of the probes were excluded from the study, since their magnitude would have been insignificant compared to other error components.

4.3. Angular position error of the probes

The uncertainty of the amplitudes of the odd harmonic components was mainly affected by the angular position error of the probes. However, the phases of both even and odd components produced significant uncertainties, the highest being c. 14° . The angular position error, especially of S2 and S3, made a main contribution to the overall uncertainty of the method.

4.4. Vertical position error of the frame

The vertical position error produced similar level amplitude uncertainties as the angular position error of the sensors. In this case, the highest phase uncertainty was detected (c. 26°). However, only the odd harmonic components were affected with the vertical position error being the only error source.

4.5. Temperature error

Temperature error had a very small effect on the amplitude uncertainties. The effect was mainly seen in the lower harmonics. However, the highest and almost only significant phase uncertainty (c. 5°) was detected in the 2nd harmonic component, which was an important contribution to the overall uncertainty of the method.

The short measurement time, controlled measurement environment

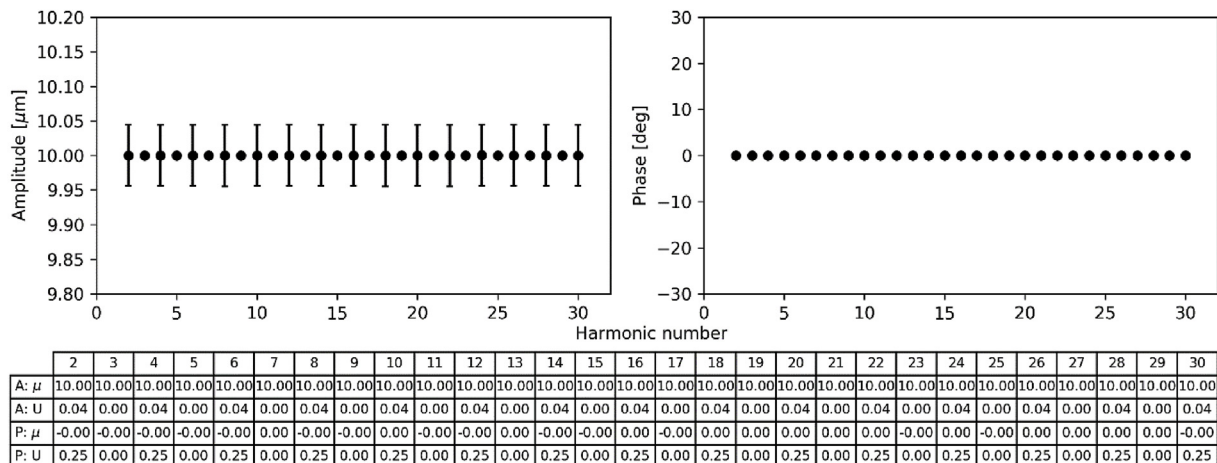


Fig. 11. Simulation output with only S4 scale error (1 μm STD) and 100000 iterations. Other error sources were set to zero. Phases are normalized, i.e., the difference between the mean value and the original value is shown.

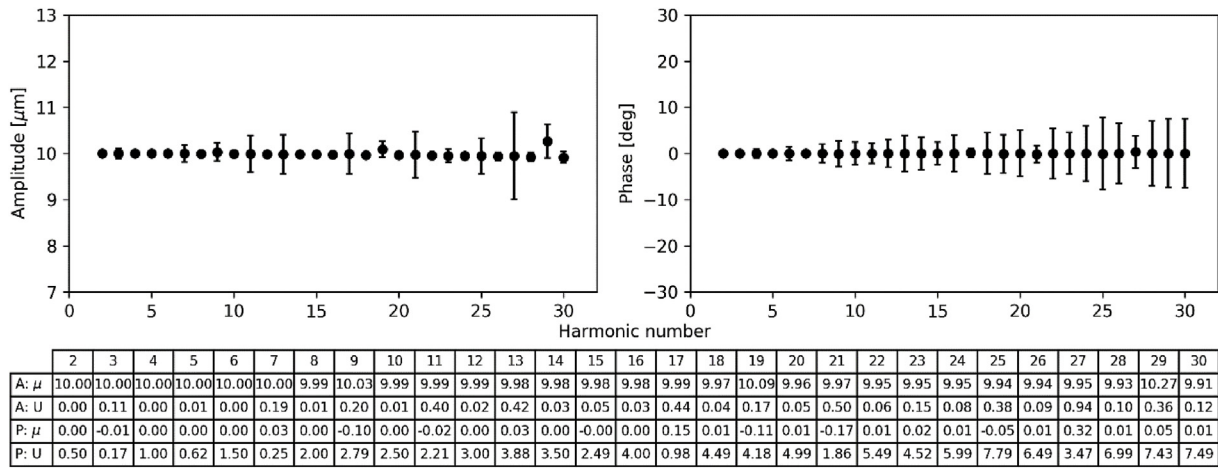


Fig. 12. Simulation output with only S1 angular position error (0.5° STD) and 100000 iterations. Other error sources were set to zero. Phases are normalized, i.e., the difference between the mean value and the original value is shown.

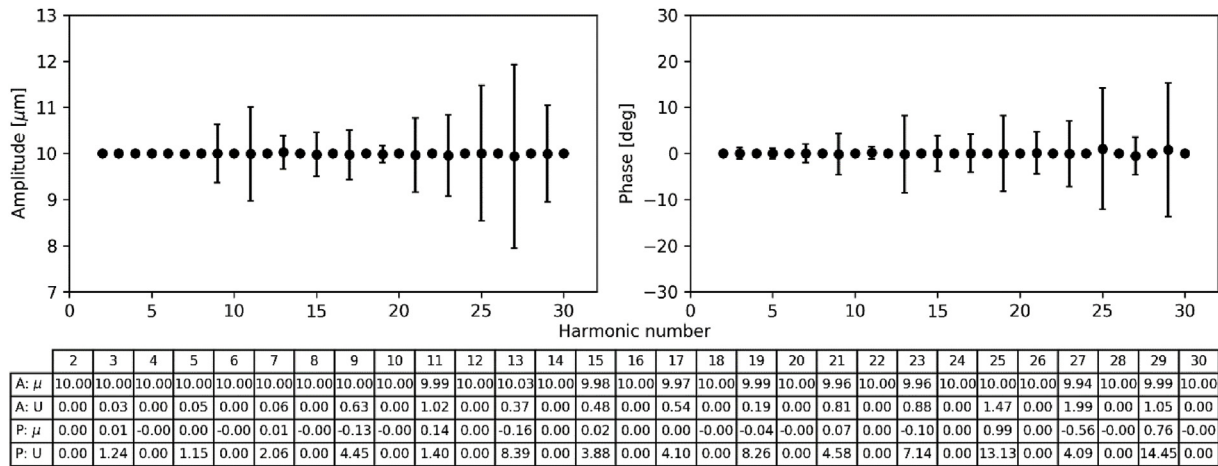


Fig. 13. Simulation with output only S2 angular position error (0.5° STD) and 100000 iterations. Other error sources were set to zero. Phases are normalized, i.e., the difference between the mean value and the original value is shown.

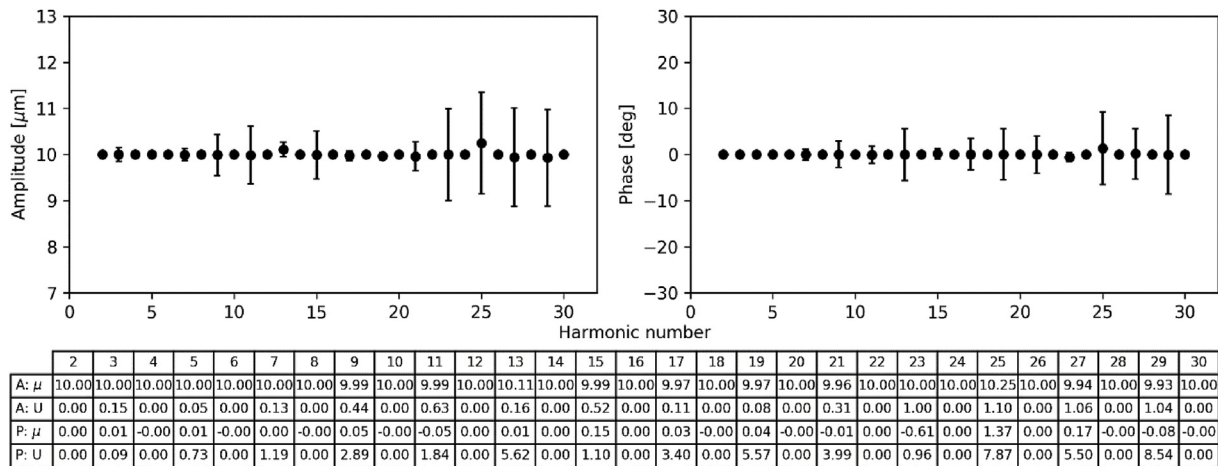


Fig. 14. Simulation output with only S3 angular position error (0.5° STD) and 100000 iterations. Other error sources were set to zero. Phases are normalized, i.e., the difference between the mean value and the original value is shown.

and, in typical applications thermalized workpieces mitigate the effect of the temperature on the overall uncertainty of the measurement method.

4.6. Random phases

The results produced by the randomly generated phases of the harmonic components in the input profile showed that the measurement method or its uncertainties were not sensitive to the phase angles

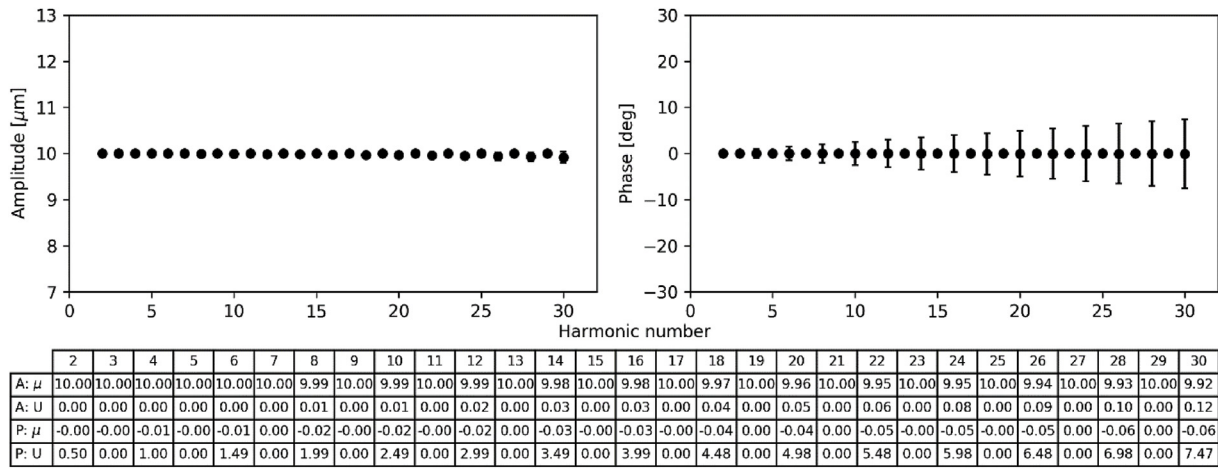


Fig. 15. Simulation output with only S4 angular position error (0.5° STD) and 100000 iterations. Other error sources were set to zero. Phases are normalized, i.e., the difference between the mean value and the original value is shown.

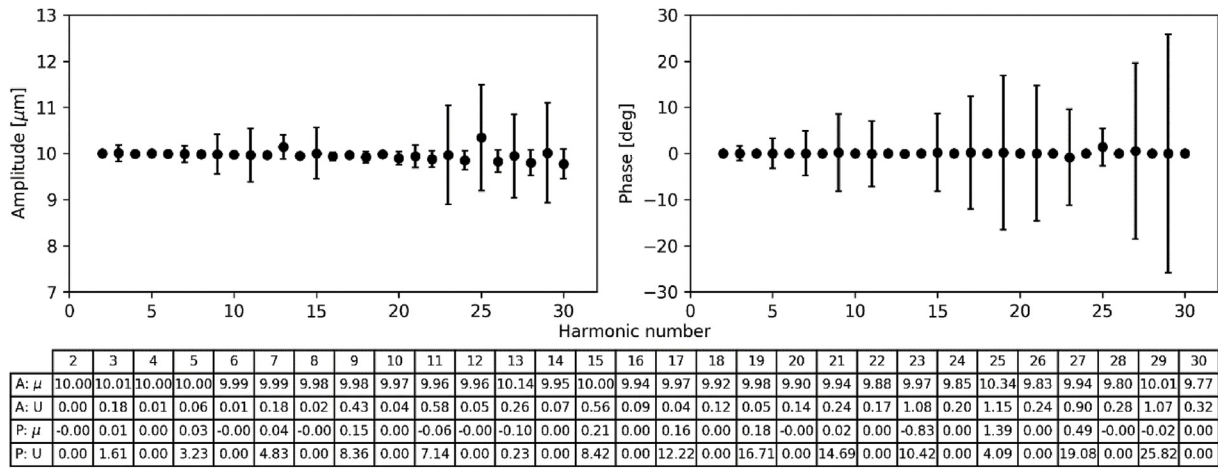


Fig. 16. Simulation output with only vertical position error (0.5 mm STD) and 100000 iterations. Other error sources were set to zero. Phases are normalized, i.e., the difference between the mean value and the original value is shown.

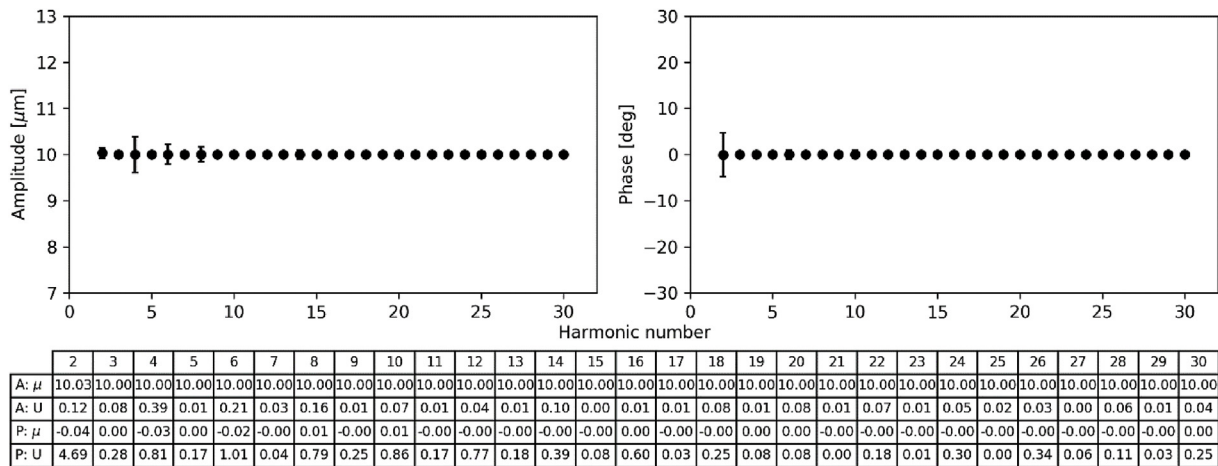
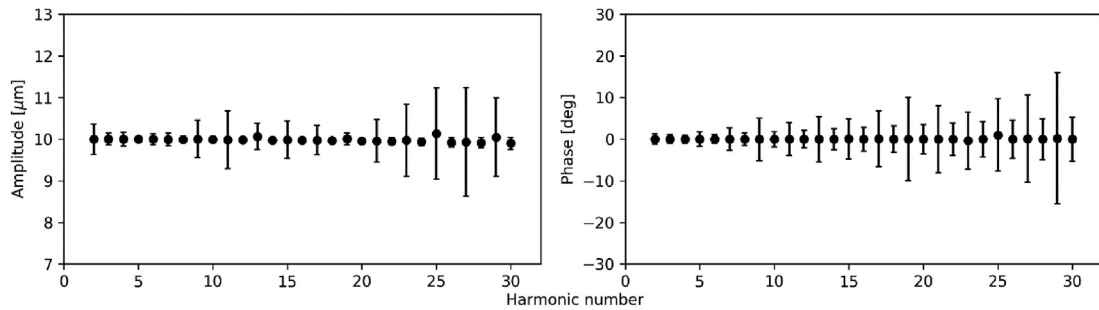


Fig. 17. Simulation output with only thermal error (1.0 °C STD) and 100000 iterations. Other error sources were set to zero. Phases are normalized, i.e., the difference between the mean value and the original value is shown.

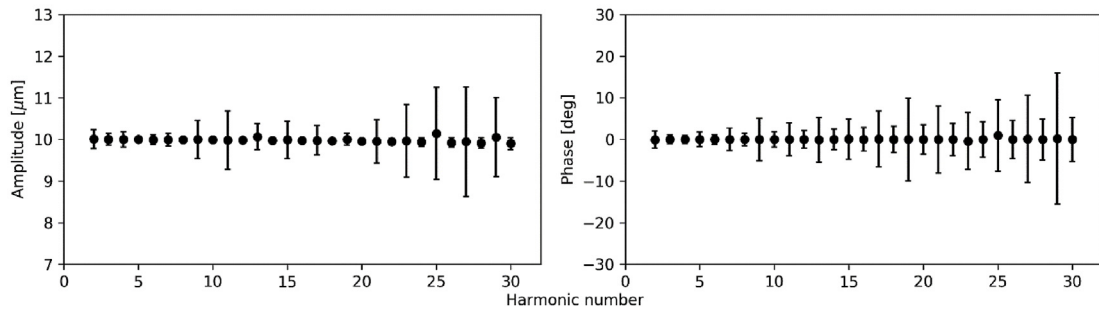
of the harmonic components. This supports the assumption that the overall uncertainty of the method is insensitive to the actual roundness profile that is being measured. No notable differences were found.

4.7. Limitations

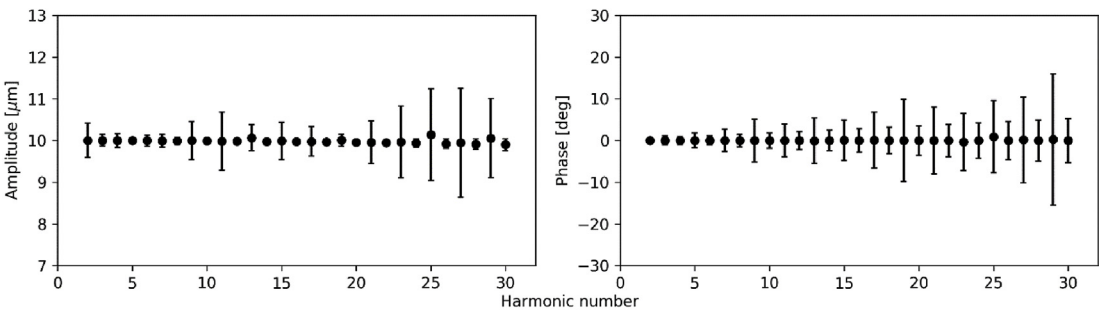
The Monte Carlo simulation based uncertainty evaluation may average the errors. The error source may not be as normally distributed as assumed and the zero expectation values may be erroneous [32]. To



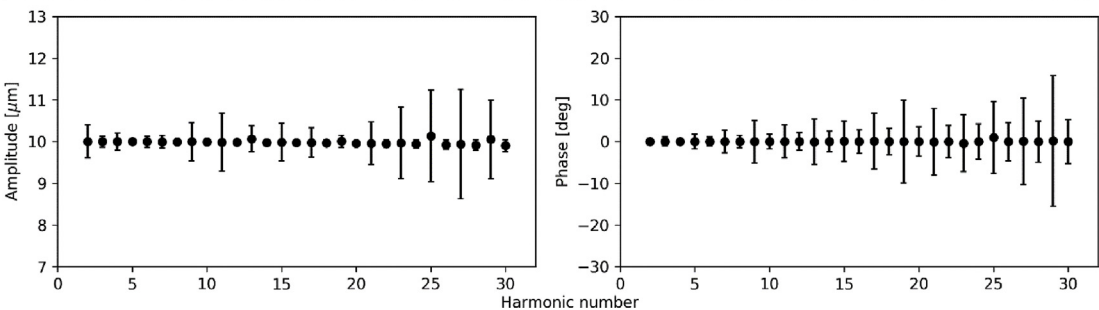
	2	3	4	5	6	7	8	9	10	11	12	13	14	15	16	17	18	19	20	21	22	23	24	25	26	27	28	29	30
A: μ	10.00	10.00	10.00	10.00	10.00	10.00	9.99	10.00	9.99	9.99	9.98	10.06	9.98	9.99	9.97	9.97	9.96	10.01	9.96	9.96	9.95	9.97	9.94	10.13	9.93	9.93	9.91	10.05	9.90
A: U	0.37	0.14	0.17	0.05	0.13	0.15	0.08	0.46	0.05	0.69	0.07	0.31	0.04	0.45	0.04	0.36	0.07	0.15	0.06	0.51	0.09	0.86	0.09	1.10	0.11	1.31	0.13	0.95	0.14
P: μ	0.05	0.01	-0.02	0.01	0.00	0.02	-0.00	-0.01	-0.00	-0.00	-0.00	-0.03	-0.00	0.09	-0.00	0.08	-0.01	0.02	-0.01	-0.03	-0.01	-0.37	-0.01	1.00	-0.01	0.12	-0.01	0.20	-0.01
P: U	1.21	1.04	1.01	1.79	1.09	2.71	1.47	5.16	1.82	3.95	2.13	5.41	2.50	4.85	2.85	6.71	3.19	9.97	3.55	8.05	3.90	6.85	4.25	8.65	4.61	10.40	4.96	15.78	5.31



	2	3	4	5	6	7	8	9	10	11	12	13	14	15	16	17	18	19	20	21	22	23	24	25	26	27	28	29	30
A: μ	10.01	10.00	10.00	10.00	10.00	9.99	9.99	10.00	9.99	9.98	9.98	10.06	9.98	9.99	9.97	9.98	9.96	10.01	9.96	9.96	9.95	9.97	9.94	10.14	9.92	9.95	9.91	10.05	9.90
A: U	0.22	0.14	0.18	0.05	0.11	0.15	0.02	0.46	0.04	0.70	0.06	0.31	0.07	0.45	0.06	0.36	0.06	0.14	0.07	0.51	0.08	0.87	0.10	1.11	0.11	1.31	0.12	0.95	0.14
P: μ	-0.05	0.00	-0.01	0.01	-0.00	0.02	0.00	-0.01	0.00	0.00	0.00	-0.07	0.00	0.09	0.01	0.08	0.01	0.01	0.01	-0.03	0.01	-0.39	0.01	0.94	0.01	0.12	0.01	0.18	0.01
P: U	2.04	1.04	0.91	1.79	1.16	2.71	1.53	5.15	1.82	3.95	2.13	5.40	2.47	4.85	2.83	6.71	3.18	9.95	3.53	8.06	3.88	6.85	4.23	8.61	4.58	10.42	4.94	15.74	5.29



	2	3	4	5	6	7	8	9	10	11	12	13	14	15	16	17	18	19	20	21	22	23	24	25	26	27	28	29	30
A: μ	10.00	10.00	10.00	10.00	10.00	9.99	9.99	10.00	9.99	9.98	9.98	10.06	9.98	9.99	9.97	9.98	9.96	10.01	9.96	9.96	9.95	9.96	9.94	10.14	9.93	9.94	9.91	10.05	9.90
A: U	0.41	0.14	0.17	0.05	0.14	0.15	0.09	0.46	0.05	0.69	0.07	0.31	0.07	0.45	0.07	0.35	0.07	0.14	0.08	0.51	0.08	0.86	0.10	1.10	0.11	1.31	0.13	0.95	0.14
P: μ	-0.02	0.01	0.01	0.01	-0.01	0.02	-0.01	0.00	-0.01	0.01	-0.01	-0.08	-0.01	0.10	-0.01	0.10	-0.02	0.04	-0.02	-0.01	-0.02	-0.38	-0.02	0.93	-0.02	0.15	-0.02	0.23	-0.03
P: U	0.53	1.04	1.01	1.78	1.07	2.69	1.46	5.13	1.81	3.93	2.13	5.41	2.48	4.82	2.83	6.67	3.18	9.91	3.54	8.00	3.89	6.82	4.24	8.63	4.59	10.35	4.95	15.67	5.30



	2	3	4	5	6	7	8	9	10	11	12	13	14	15	16	17	18	19	20	21	22	23	24	25	26	27	28	29	30
A: μ	10.00	10.00	10.00	10.00	10.00	9.99	9.99	10.00	9.99	9.98	9.98	10.06	9.98	9.99	9.97	9.98	9.96	10.01	9.96	9.96	9.95	9.97	9.94	10.13	9.93	9.94	9.91	10.05	9.90
A: U	0.40	0.13	0.21	0.05	0.14	0.15	0.06	0.46	0.07	0.69	0.05	0.31	0.07	0.45	0.04	0.35	0.07	0.14	0.07	0.51	0.09	0.86	0.10	1.10	0.11	1.31	0.12	0.94	0.14
P: μ	-0.03	0.00	-0.00	0.00	0.00	0.01	0.01	-0.02	0.01	-0.01	0.00	-0.06	0.01	0.08	0.01	0.07	0.01	-0.00	0.01	-0.05	0.01	-0.39	0.01	0.94	0.01	0.10	0.01	0.17	0.01
P: U	0.84	1.05	0.75	1.78	1.07	2.70	1.51	5.13	1.80	3.93	2.15	5.39	2.48	4.82	2.85	6.68	3.19	9.92	3.54	8.01	3.89	6.83	4.25	8.61	4.60	10.36	4.96	15.70	5.31

Fig. 18. Four simulation outputs with randomly generated phases of the input profile. All the error sources were used (quantities presented in Table 1) and number of iterations was 10000.

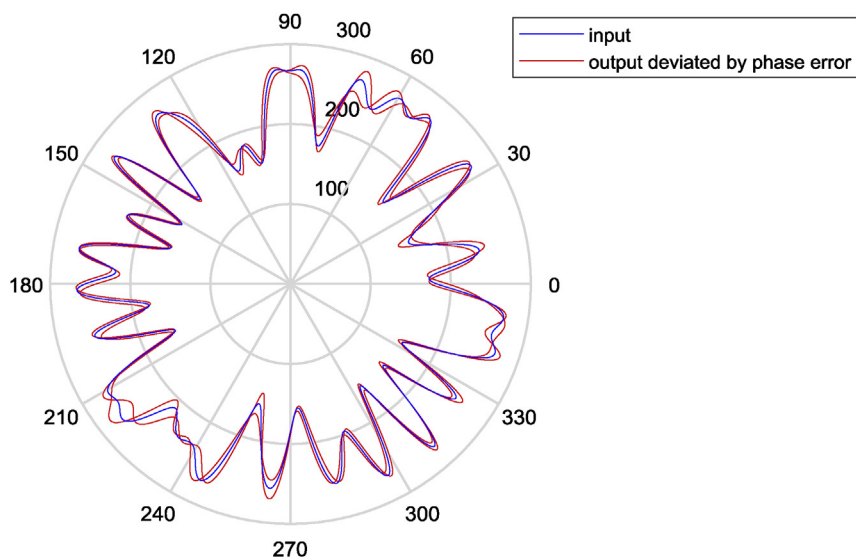


Fig. 19. Example of the phase uncertainty distorted roundness profiles. The blue input roundness profile is the same as in Fig. 5. A). The red curves represent roundness profiles, which were reproduced by using the standard amplitude $10\ \mu\text{m}$ for all the harmonic components and using the phases interpreted by the algorithm in two Monte Carlo iterations in case of “vertical position error of the frame”. (For interpretation of the references to colour in this figure legend, the reader is referred to the Web version of this article.)

resolve this problem, autocorrelation and cross correlation studies between different sensitivity cases should be undertaken.

The error distribution values were based on the best hypothesis of the authors. The values may have been erroneous and there may be other, more significant error sources not presented in this study.

5. Conclusion

The measurement uncertainty is an essential property of a measurement method. This present study investigated the multiple possible error sources and their influence on the overall uncertainty of the detected amplitudes and phases of the harmonic components of the roundness profile were investigated. The four-point roundness measurement method was shown to be robust and feasible in both industrial and scientific use. However, vibration and insufficient stiffness of the measurement device may increase the overall uncertainty of the method in industrial usage.

Below the 10th harmonic component of the roundness profile, both the amplitude and phase uncertainties were on an acceptable level with the proposed error contributions. The method is considered valid for the presented application, where the roundness profile of the bearing inner ring installed on the rotor shaft is measured and analysed to determine its contribution to the vibration excitation.

The uncertainty of the phase was found to be highly dependent on the angular position of the sensors as well as the vertical position of the measurement frame. Relatively high phase uncertainties were detected, especially considering the higher harmonic components (over the 10th), albeit the uncertainties in the actual workpiece coordinate system remain minor. Consequently, as a result of the present study, the accurate angular positioning of the sensors and vertical positioning of the frame should be emphasized, since they seem to have the greatest contribution to the overall uncertainty of the measurement method. The angular error of the sensor positions is more a measurement frame manufacturing related problem and is avoidable with a strict angular tolerance. The vertical error of the frame is more dependent on the measurement setup and the operator. Here, a certain level of automation can provide a reliable solution for the correct vertical position of the frame.

The problems related to the higher order harmonic component phase uncertainty detected in the present study are considered significant and their influence on the precision manufacturing accuracy has to be investigated. Fig. 19 presents an example of the possible measured roundness profiles, when only the phase error is considered. Significant deviations from the input profile are observable. For

example, in some applications, the bearing inner ring roundness profile is optimized through the predictive grinding [12] of the installation shaft of the rotor. Here the phase error may cause severe problems to the manufacturing accuracy due to erroneous roundness profile feedback. In an extreme situation, due to phase error, the amplitude of certain harmonic components may become two-fold after the grinding with the feedback information.

Acknowledgements

This work was supported by Academy of Finland (ViDROM, grant number 277964) and EMRP (DriveTrain, grant number ENG56-REG1). The authors would like to express their gratitude to M.Sc. (Tech.) Ville Klar for the assistance with the simulation software.

References

- [1] Heikkinen JE, Ghalamchi B, Viitala R, Sopanen J, Juhanko J, Mikkola A, Kuosmanen P. Vibration analysis of paper machine’s asymmetric tube roll supported by spherical roller bearings. *Mech Syst Signal Process* 2018;104:688–704 <https://doi.org/10.1016/j.ymssp.2017.11.030>.
- [2] Viitala R, Widmaier T, Kuosmanen P. Subcritical vibrations of a large flexible rotor efficiently reduced by modifying the bearing inner ring roundness profile. *Mech Syst Signal Process* 2018;110:42–58 <https://doi.org/10.1016/j.ymssp.2018.03.010>.
- [3] International Organization of Standardization. ISO 12181-1:2011 Geometrical product specifications (GPS) - Roundness - Part 1: vocabulary and parameters of roundness. 2011. p. 13.
- [4] International Organization of Standardization. ISO 12181-2:2011 Geometrical product specifications (GPS) - Roundness - Part 2. Specification operators; 2011. p. 9.
- [5] Haitjema H, Bosse H, Frennberg M, Sacconi A, Thalmann R. International comparison of roundness profiles with nanometric accuracy. *Metrologia* 1996;33:67–73 <https://doi.org/10.1088/0026-1394/33/1/9>.
- [6] Neugebauer M. Uncertainty analysis for roundness measurements by the example of measurements on a glass hemisphere. *Meas Sci Technol* 2001;12:68–76 <https://doi.org/10.1088/0957-0233/12/1/309>.
- [7] Thalmann R, Spiller J, Küng A, Jusko O. Calibration of flick standards. *Meas Sci Technol* 2012;23:94008 <https://doi.org/10.1088/0957-0233/23/9/094008>.
- [8] Ozono S. On a new method of roundness measurement based on the three points method. *Proc Int Confer Prod Eng Tokyo* 1974:457–62.
- [9] Juhanko J. Dynamic geometry of a rotating paper machine roll Aalto University Publication Series 117/2011978-952-60-4363-0; 2011. p. 172. Doctoral dissertation.
- [10] Kiviluoma P. Method and device for in situ runout measurement of calender thermo rolls Espoo: Helsinki University of Technology 978-952-248-259-4; 2009. Doctoral dissertation.
- [11] Kotamaki MJ. In situ measurement and compensation control in external grinding of large cylinders. Helsinki: Acta Polytechnica Scandinavica, Mechanical Engineering Series 121; 1998. p. 123.
- [12] Kuosmanen P. Predictive 3D roll grinding method for reducing paper quality variations in coating machines Doctoral dissertation Espoo: Helsinki University of Technology 951-22-7014-5; 2004 Publications in Machine Design 2/2004.

- [13] Widmaier T. Optimisation of the roll geometry for production conditions Aalto University Publication Series 156/2012978-952-60-4878-9; 2012. p. 184. Doctoral dissertation.
- [14] Janssen M, Schellekens P, De Veer B. Advanced spindle runout-roundness separation method. *Adv Math Computational Tools Metrology V 2001:212–9*https://doi.org/10.1142/9789812811684_0024.
- [15] BIPM, IEC, IFCC, ILAC, ISO, IUPAC, IUPAP, OIML. Guide to the expression of uncertainty in measurement (GUM 1995 with minor corrections). International Organization for Standardization, JCGM; 2010.
- [16] BIPM, IEC, IFCC, ILAC, ISO, IUPAC, IUPAP, OIML. Evaluation of measurement data — supplement 1 to the Guide to the expression of uncertainty in measurement — propagation of distributions using a Monte Carlo method. International Organization for Standardization, JCGM; 2008.
- [17] Brizard M, Megharfi M, Verdier C. Absolute falling-ball viscometer: evaluation of measurement uncertainty. *Metrologia* 2005;42:298–303<https://doi.org/10.1088/0026-1394/42/4/015>.
- [18] Morel M, Haitjema H. Task specific uncertainty estimation for roundness measurement. Proc. of the 3rd euspen international conference, eindhoven, The Netherlands, May 26th-30th, 2002. 2002. p. 513–6.
- [19] Wübbeler G, Krystek M, Elster C. Evaluation of measurement uncertainty and its numerical calculation by a Monte Carlo method. *Meas Sci Technol* 2008;19:84009<https://doi.org/10.1088/0957-0233/19/8/084009>.
- [20] Cooley JW, Tukey JW. An algorithm for the machine calculation of complex Fourier series. *Math Comput* 1965;19:297–301.
- [21] Mosier-Boss PA, Lieberman SH, Newbery R. Fluorescence rejection in Raman spectroscopy by shifted-spectra, edge detection, and FFT filtering techniques. *Appl Spectrosc* 1995;49:630–8.
- [22] Muralikrishnan B, Raja J. Computational surface and roundness metrology vol. 262. Springer Science & Business Media 978-1-84800-296-8; 2008.
- [23] Whitehouse DJ. Handbook of surface metrology. CRC Press; 1994.
- [24] Widmaier T, Hemming B, Juhanko J, Kuosmanen P, Esala P, Lassila A, Laukkanen P, Haikio J. Application of Monte Carlo simulation for estimation of uncertainty of four-point roundness measurements of rolls. *Precis Eng* 2016;48:181–90<https://doi.org/10.1016/j.precisioneng.2016.12.001>.
- [25] Kato H, Nakano Y, Nomura Y. Development of in-situ measuring system of circularity in precision cylindrical grinding. *Bull Jpn Soc Precis Eng* 1990;24:130–5.
- [26] Kato H, Sone RY, Nomura Y. In-situ measuring system of circularity using an industrial robot and a piezoactuator. *Int J Jpn Soc Precis Eng* 1991;25:130–5.
- [27] Väänänen P. Turning of flexible rotor by high precision circularity profile measurement and active chatter compensation Espoo: Helsinki University of Technology; 1993. Licentiate's thesis.
- [28] Haitjema H. Revisiting the multi-step method: enhanced error separation and reduced amount of measurements. *CIRP Annals* 2015;64:491–4<https://doi.org/10.1016/J.CIRP.2015.03.00>.
- [29] Hemming B, Widmaier T, Palosuo I, Esala V-P, Laukkanen P, Lillepea L, Simson K, Brabandt D, Haikio J. Traceability for roundness measurements of rolls. 9th international DAAAM Baltic conference industrial engineering 24-26 April 2014. 2014. p. 232–7. Tallinn, Estonia.
- [30] Widmaier T, Kuosmanen P, Hemming B, Esala VP, Brabandt D, Haikio J. New material standards for traceability of roundness measurements of large scale rotors. Proceedings of the 58th ilmenau scientific colloquium. 2014. p. 9.
- [31] Harris PM, Cox MG. On a Monte Carlo method for measurement uncertainty evaluation and its implementation. *Metrologia* 2014;51:176–82<https://doi.org/10.1088/0026-1394/51/4/S176>.
- [32] van Dorp B, Delbressine FLM, Haitjema H, Schellekens PHJ. Traceability of CMM measurements. Proceedings of American Society for Precision Engineering - ASPE annual meeting, Monterey, USA. 1999.